THE ASTRONOMICAL JOURNAL VOLUME 105, NUMBER 3 MARCH 1993

HYPERFINE STRUCTURE OF HCN $J=1$–0 AND IMPLIED PHYSICAL INFORMATION CONCERNING NGC 7538 IRS1

Y. X. CAO AND Q. ZENG

Purple Mountain Observatory, Nanjing 210008, People's Republic of China

S. DEGUCHI, O. KAMEYA,[1] AND N. KAIFU[2]

Nobeyama Radio Observatory, Minamisaku, Minamimaki, Nagano, 384-13, Japan

Received 8 May 1992; revised 26 October 1992

ABSTRACT

The so-called intensity anomalies of hyperfine components of HCN($v=0$, $J=1$–0) in the NGC 7538 molecular cloud are studied with a high resolution spectrometer. The measured intensity ratio $R_{02}=T_a^*(F=0\text{–}1)/T_a^*(F=2\text{–}1)$ is clearly larger than the value 0.2, which is expected under the optically thin local thermodynamic equilibrium (LTE) condition, and the ratio $R_{12}=T_a^*(F=1\text{–}1)/T_a^*(F=2\text{–}1)$ smaller than the LTE value 0.6 at most of the observed positions. Radiative transfer calculations were performed using the large velocity gradient (LVG) model with a spherically symmetric velocity field. The line overlaps have also been taken into account. The analysis of the observational data shows that the three hyperfine components of the $J=1$–0 transition are optically thick. While the optical depths of $F=2$–1 and $F=1$–1 are much larger than that of $F=0$–1 hyperfine component, the scattering effect must be taken into account. The stronger two hyperfine components, $F=2$–1, and $F=1$–1, are formed in the envelope with the average hydrogen density 1.6×10^4 cm^{-3}, but the thinner $F=0$–1 hyperfine component in the core and in the envelope. The excitation temperatures of the three hyperfine components are different and the LTE assumption for the HCN hyperfine intensity ratio is unrealistic.

1. INTRODUCTION

The interstellar molecule HCN is characterized by its high dipole moment and its hyperfine structure. Many observations show that the relative intensity ratios of the three hyperfine components of the $v=0$, $J=1$–0 transition, i.e., $R_{02}=T_a^*(F=0\text{–}1)/T_a^*(F=2\text{–}1)$ and $R_{12}=T_a^*(F=1\text{–}1)/T_a^*(F=2\text{–}1)$, are often different from the local thermodynamic equilibrium (LTE) values i.e., 0.2 and 0.6, respectively, under optically thin conditions. This problem was first theoretically tackled by Kwan (1974). In order to expound the so-called anomalies, Guilloteau & Baudry (1981) developed the thermal overlap model, which originated from Gottlieb *et al.* (1975). According to this model, they accredited $R_{02}<0.2$, and $R_{12}<0.6$ to the overlap of the $J=2$–1 hyperfine transitions, which leads to the overpopulation in the level $J=1$, $F=2$. However, Walmsley *et al.* (1982) broached some doubts about the thermal overlap model when they observed toward TMC-1. In their observations, the emission intensity of the $F=0$–1 hyperfine component was the strongest in three hyperfine components, and could not be interpreted by thermal overlap. Zinchenko & Pirogov (1987) elucidated the anomalous phenomenon by the LVG model. But those investigations still could not account for the fact that R_{02} is often larger than 0.2. Considering the noticeable differences between the opacities of the hyperfine satellites, $F=2$–1 and $F=1$–1, and that of $F=0$–1, Cernicharo *et al.* (1984) suggested a scattering model; photons of two optically thick $F=2$–1 and $F=1$–1 components are scattered more than photons of the optically thin $F=0$–1 component are.

We report here the result of our measurements of HCN hyperfine ratios toward the NGC 7538 molecular cloud. The intensity anomalies appear in the hyperfine components strongly in this cloud. Pratap *et al.* (1989,1990) also mapped emission of the HCN $J=1$–0 transition toward NGC 7538 IRS1 with the BIMA millimeterwave interferometer. Their intention was to map the high density clumps around IRS1 which were caused by the expansion of the H II region. We are more interested in the large scale structure of intensity anomalies of HCN hyperfine components. In order to explain the measured results, the LVG model is adopted. The line overlap effect between the hyperfine components and the scattering effect are also considered. The physical condition of the NGC 7538 molecular cloud, especially around IRS1, is elucidated on the basis of observations of hyperfine ratios.

2. OBSERVATIONS

The observations of HCN $v=0$, $J=1$–0 transitions at 88.631 GHz were made on 3 May 1990, with the 45 m telescope at Nobeyama Radio Observatory. The half-power beam width (HPBW) was 22″, and the main-beam and aperture efficiencies were 0.68 and 0.5, respectively. We used a cooled receiver with a SIS mixer noise temperature of 480 K (a single sideband including the atmo-

[1]Present address: Mizusawa Astrogeodynamics Observatory, Mizusawa, Iwate, 023, Japan.

[2]Present address: National Astronomical Observatory, Mitaka, Tokyo 181, Japan.

 0004-6256/93/031027-06$00.90

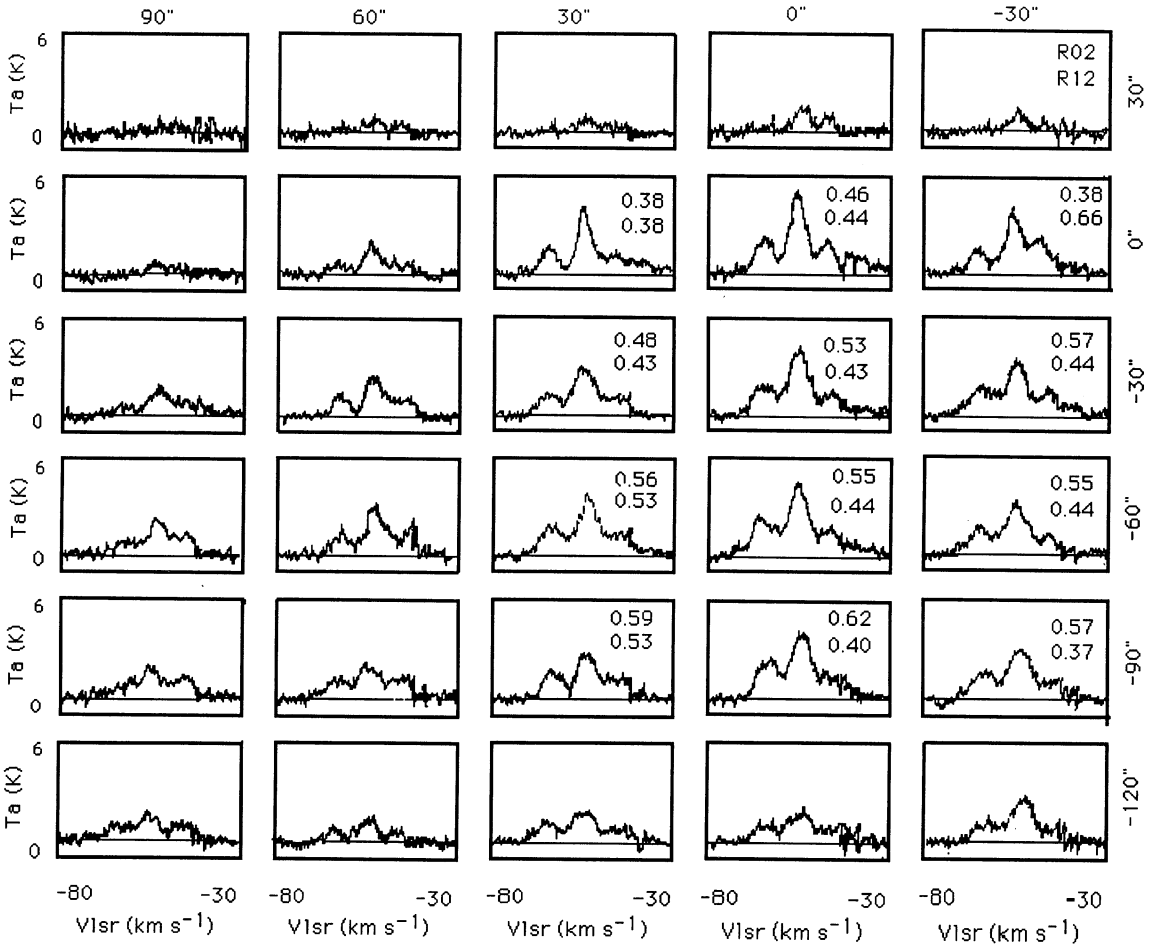

FIG. 1. Profile maps of the HCN (v=0,J=1–0) emission in NGC 7538. The origin is set at IRS1 [R.A.(1950)=$23^h11^m36.8^s$,Dec.(1950) =61°11′48″]. The spectra are arranged along the right ascencion and declination directions with a separation of 30″. The hyperfine intensity ratios, R_{02}(upper) and R_{12}(lower) at each position, are indicated at the top right corner in each panel. Bad channels in the spectrometer appeared at $V_{lsr}=-45$ to -43 km s^{-1} and were taken out.

spheric noise and antenna ohmic loss). Mapping observation interval was 30″, and a 150″×120″ area including IRS1 and IRS11 was mapped. The origin of the map was set at the position of IRS1 [R.A.(1950)=$23^h11^m36.8^s$ and Dec.(1950)=61°11′48″]. Here, we use the offset (ΔRA,ΔDEC) from the origin. The pointing accuracy was checked every two hours by observing the SiO maser from R Cas and a mean position error was approximately 7″ during the observations.

Twelve arrays of 2048-channel acousto-optical spectrometer (AOS) were used for the backends with a frequency resolution 37 kHz(0.125 km s^{-1}) for the high resolution arrays and a resolution 250 kHz(0.88 km s^{-1}) for the low resolution arrays. In order to decrease the noise, seven channels were combined for the data reduction of the high resolution array. The observed spectra of the J=1–0 transition are shown in Fig. 1. The ratios of the hyperfine components, R_{02} and R_{12}, are also shown at the top right corner of the individual panels in Fig. 1. The ratios, R_{02} and R_{12}, have been obtained by fitting the spectra of three hyperfine components with three Gaussians and the peak values of the Gaussians are taken as the line intensities. The linewidth of a single component varies from 5.5 to 3.8 km s^{-1} with the declination, but we have not found a noticeable variation of halfwidths among hyperfine components; we have assumed that the line widths of hyperfine components are equal at each position. Apparently, the intensity ratio indicates a deviation from thermal equilibrium. For instance, at the origin (Fig. 2), R_{02}=0.46 and R_{12}=0.44.

Figure 3 shows contour maps of the integrated antenna temperature of F=0–1 (thin solid curve), F=2–1 (thick solid curve), and F=1–1 (dot). High intensity parts are separated into two regions: one near IRS1 at (0″,0″) and another near IRS11 at (−12″,−70″). From this figure, we can see the integrated antenna temperature of F=0–1 is stronger than F=1–1 around IRS1 and IRS11.

3. MODEL AND CALCULATIONS

In order to interpret the observational results, we have performed the radiative transfer calculation with the pho-

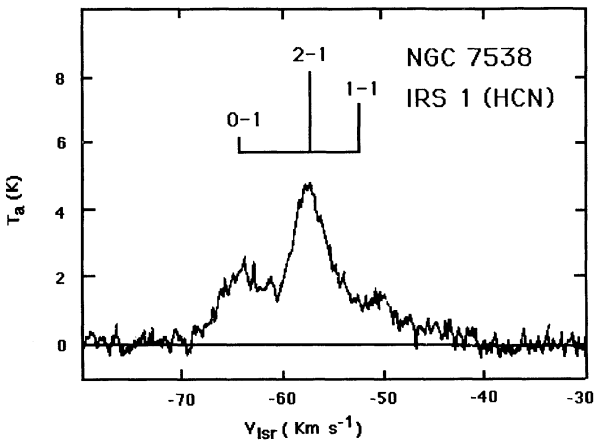

FIG. 2. The spectrum of the HCN (v=0,J=1–0) at IRS1 in NGC 7538 [R.A.(1950)=$23^h11^m36.8^s$,Dec.(1950)=61°11′48″]. [The quality of this spectrum is improved to the spectrum in Fig. 1 at the same position by adding a few more scans taken for calibrations.]

ton escape probability method (Goldreich & Kwan 1974). We assume that the radiation from IRS1 and IRS11 is absorbed by the dust of the outer envelope. HCN molecules are exposed in the radiation field of the dust and the 3 K microwave background radiation. The statistical equilibrium equation for the level l is

$$\sum_i n(i)C(i,l)+\sum_i n(i)B(i,l)U(i,l)+\sum_i n(i)A(i,l)$$
$$=\sum_i n(l)C(l,i)+\sum_i n(l)B(l,i)U(l,i)+\sum_i n(l)A(l,i), \quad (1)$$

where $n(i)$ is the population of HCN at the level i, $A(i,l)$ and $B(i,l)$ the *Einstein A* and B coefficients, $C(i,l)$ the collisional transition rate, $U(i,l)$ the radiation density of

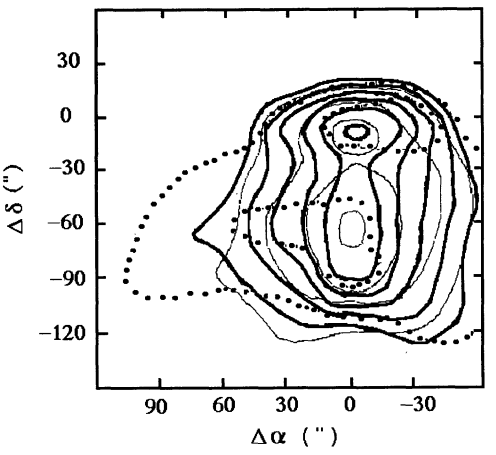

FIG. 3. Contour map of the integrated intensity $\int T_R^* dv$ for the HCN v=0, J=1–0 transition: the F=2–1 component (solid thick line), F=0–1 (thin line), and F=1–1 (dot). The origin is at IRS1. The lowest level is 5 K km s^{-1} and the interval is 2 K km s^{-1}. The positions of IRS1 and IRS11 are (0″,0″) and (−12″,−70″), respectively.

the radiative transition from i to l. We got the radiative transition rates from Guilloteau & Baudry (1981) as

$$A(jf-j'f')=64\pi\nu^3_{jf-j'f'}/(3hc^3)(2f'+1)$$
$$\times\begin{Bmatrix} j & f & 1 \\ j' & f' & 1\end{Bmatrix}|d_{jf-j'f'}|^2, \quad (2)$$

$$B(jf-j'f')=c^3/(8\pi h\nu^3_{jf-j'f'})A_{jf-j'f'}, \quad (3)$$

where h is the Planck constant, c the velocity of light, and $\nu_{jf-j'f'}$ the frequency of the transition from (jf) to ($j'f'$). Here, { } is the Wigner's 6-j symbol, and $d_{jf-j'f'}$ the dipole moment. The collisional transition rate of HCN with H_2 is quite important to calculate the level populations and several studies has been made on this topic (Varshalovich & Khersonsky 1977; Monteiro & Stutzki 1986). In this paper, we adopt the collisional transition rate between the hyperfine levels from Varshalovich & Khersonsky 1977 as

$$W_{jf-j'f'}(T,\Delta E)$$
$$=(2f'+1)(2j'+1)(2j+1)$$
$$\times\sum\begin{pmatrix} j' & s & j \\ 0 & 0 & 0\end{pmatrix}^2\begin{Bmatrix} f & f' & s \\ j' & j & 1\end{Bmatrix}W_s(T,\Delta E), \quad (4)$$

where

$$W_s(T,\Delta E)=w_s(T/T_s)^m\exp[-(T/T_s)^n] \quad (5)$$

and w_s, m, n, and T_s are parameters, and ( ) is the Wigner's 3-j symbol. The radiation field $U(i,l)$ is given (Zinchenko & Pirogov 1987; Zeng & Lo 1988) by

$$U(i,l)=\left\{\sum_{i'l'}(2h\nu^3_{i'l'}/c)\tau_{i'l'}[\exp(h\nu_{i'l'}/(kT_{ex})-1)]^{-1}\right\}\Big/$$
$$\left[\sum_{i'l'}\tau_{i'l'}\right]+2h\nu^3_{il}\beta_{il}\{[\exp(h\nu_{il}/(kT_{bb})-1)]^{-1}$$
$$+\tau_{il}[\exp(h\nu_{il}/(kT_{bb})-1)]^{-1}\}, \quad (6)$$

where k is the Boltzmann constant, T_{bb} the temperature of the microwave background radiation (=2.7 K), T_d the temperature of dust radiation (taken as 40 K; Thronson & Harper 1979), and τ_{il} the dust opacity at the frequency ν_{il}, $T_{ex}(i,l)$ the excitation temperature between the levels i and l. Here the summation in Eq. (6) is taken over those components of overlapped transitions for which the frequencies ν_{il} and $\nu_{i'l'}$ satisfy the condition

$$|\nu_{il}-\nu_{i'l'}|<\nu_a\Delta v/c, \quad (7)$$

where ν_a is the average frequency of ν_{il} and $\nu_{i'l'}$, and Δv is the thermal width. We take T_k=25 K, and Δv=0.22 km s^{-1}. For the grain opacity, we adopt (Thronson & Harper 1979)

$$\tau_{il}=\nu_{il}/\nu_0 \quad \text{when} \quad \nu_{il}<\nu_0,$$
$$1 \quad \text{when} \quad \nu_{il}>\nu_0, \quad (8)$$

where ν_0 is 8565 GHz. Further, β_{il}, the escape probability of photons of the transition from i to l, is

$$\beta_{jf-j'f'}=[1-\exp(-\tau^t_{jf-j'f'})]/\tau^t_{jf-j'f'} \quad (9)$$

and the total optical depth

$$\tau^t_{j'f'}=\sum_{jf-j'f'}\tau_{jf-j'f'}, \quad (10)$$

where $\tau_{jf-j'f'}$ is the optical depth of the transition from jf to $j'f'$ and the summation in Eq. (10) is taken for the overlapped components which satisfy Eq. (7). To obtain the optical depth, we employ the large velocity gradient model with velocity field $V(r)=(V/R)r$, where V and R are the expanding velocity at the boundary of the cloud and radius of the cloud. The optical depth is given as

$$\tau_{jf-j'f'}=c^3A_{jf-j'f'}/(8\pi\nu^3_{jf-j'f'})n_{jf} \times\{n_{j'f'}(2f+1)/[n_{jf}(2f'+1)]-1\}R/V. \quad (11)$$

Based on the present and the former observations (Kameya 1985; Dickel *et al.* 1981), we adopt the velocity gradient $(V/R)=1.5$ km s^{-1} pc^{-1} and the kinetic temperature 25 K. The abundance of HCN is taken as 5×10^{-9} per H_2 (Herbst & Klemperer, 1973; Schwartz *et al.* 1977; Kameya *et al.* 1986).

The frequencies of hyperfine satellites are well separated for the $J=1$–0 transitions; 1.432 MHz (4.9 km s^{-1}) between $F=1$–1 and $F=2$–1 and 2.089 MHz (7.1 km s^{-1}) between $F=2$–1 and $F=1$–0, so that, we have assumed that the hyperfine components do not overlap each other by the velocity gradient in the cloud. However, this is no longer true for the higher J transitions, for which the velocity separation between the hyperfine satellites decreases with J. For the $J=2$–1 transition, there are two pairs of closely spaced components, $F=2$–1 and $F=3$–2, and $F=2$–2 and $F=1$–0: the velocity separation of the first pair is 0.17 km s^{-1} and the second 0.4 km s^{-1}. Due to the low kinetic temperature of about 25 K (0.22 km s^{-1}), the nonlocal overlapping is insignificant (Zinchenko & Pirogov 1987). We consider thermal (local) overlapping in our model calculations. Nonlocal line overlaps (radiative interactions with the separate points in the cloud) were not considered here. [Accurate frequencies of the HCN hyperfine transitions are listed in Maki (1974) and the useful energy level diagram for the hyperfine transitions is found in Kwan (1974).]

The statistical equilibrium calculation includes 28 hyperfine levels ($J\leqslant9$). The numerical solutions are obtained by successive iterations. The numerical results are shown in Figs. 4, 5, and 6.

4. DISCUSSION

Our calculations show that, when the hydrogen density $n(H_2)\ll10^3$ cm^{-3} (or $\tau\ll1$), the excitation temperature of the hyperfine components are identical (in optically thin LTE limit; Fig. 5), and the limiting values of R_{02} and R_{12} are 0.2 and 0.6, respectively (see Fig. 4). However, the ratios R_{02} and R_{12}, and the excitation temperatures of the hyperfine components do not change monotonously with density (or optical depth). In fact, optically thin assumption can be valid only when $n(H_2)\ll10^3$ cm^{-3} (Fig. 6). The excitation temperatures of the three hyperfine components are not identical when the hydrogen density is larger than 10^4 cm^{-3} (Fig. 5) due to the differences of radiation trapping and line overlapping. Therefore, the simple LTE optically thin approximation is unrealistic in NGC 7538. When the density is near 1.5×10^5 cm^{-3}, both R_{02} and R_{12} have a minimum (Fig. 4). These are caused by the overlapping of hyperfine components of HCN. For instance, the overlapping between $F=2$–1 and $F=3$–2 of the $J=2$–1 line leads to a population transfer from the $J=1$, $F=1$ level to the $J=1$, $F=2$ level through the $J=2$, $F=2$ level due to stimulated transitions of $(J,F)=(1,1)$–$(2,2)$. Then the ratios $R_{02}=I(F=0$–$1)/I(F=2$–$1)$ and $R_{12}=I(F=1$–$1)/I(F=2$–$1)$ in the $J=1$–0 line decrease. As the hydrogen density increases further, collisional thermalization becomes effective. The hyperfine ratios R_{02} and R_{12} increase and reach to unity at 3×10^7 cm^{-3} (they tend to exceed unity at 5×10^6 cm^{-3}).

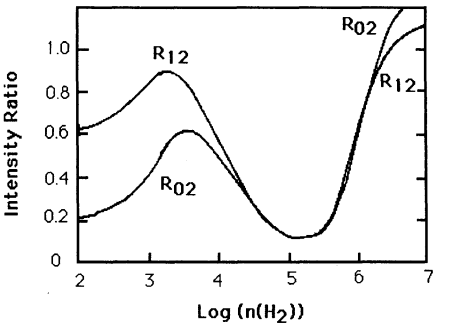

FIG. 4. Line intensity ratios R_{02} and R_{12} as a function of hydrogen number density $n(H_2)$ in unit of cm^{-3}. The abundance of HCN, the kinetic temperature and dust temperature are 5×10^{-9} per H_2, 25 and 40 K, respectively.

The values of R_{02} exceed R_{12} at most of the observed positions (Fig. 1). For example, $R_{02}=0.46$ and $R_{12}=0.44$ at the origin (IRS1). The model calculations, however, show that R_{12} is larger than R_{02} except at the high density above 1.5×10^6 cm^{-3} (Fig. 4). The ratio, R_{02}/R_{12}, takes

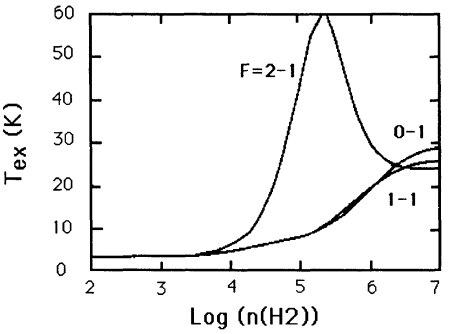

FIG. 5. The excitation temperatures of the HCN hyperfine transitions as a function of hydrogen number density. The abundance, etc. are the same as those of Fig. 4.

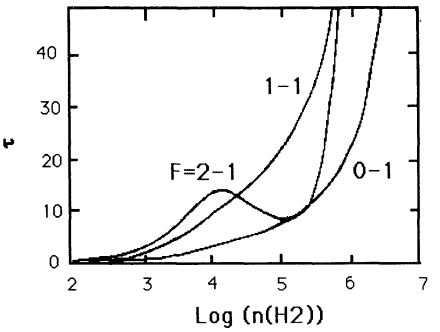

FIG. 6. The optical depths of the HCN hyperfine transitions as a function of hydrogen number density. The abundance, etc. are the same as those of Fig. 4.

the maximum value of 1.13 at the density of $\sim 10^7$ cm^{-3}. One may suppose that the anomaly, $R_{02} > R_{12}$, is explained by introducing the high density clumps in the telescope beam (22″). However, at more than a half of observed positions, this ratio, R_{02}/R_{12}, is above this maximum value. So that the anomaly ($R_{02} > R_{12}$) cannot be explained by introducing the clumps because any combination of the clumps cannot give $R_{02}/R_{12} > 1.13$.

A more plausible explanation for the anomaly is the "scattering" effect (Cernicharo *et al.* 1984). Suppose a steep density gradient is present along the line of sight. Because the optical depths of $F=2$–1 and $F=1$–1 components are much larger than that of $F=0$–1, the photons of $F=2$–1 and $F=1$–1 which are emitted in the inner region of the molecular cloud are completely absorbed and re-emitted at the outer region. On the other hand, due to the smaller opacity, the $F=0$–1 component is formed relatively at the inner part with a larger density and greater excitation temperature. The $F=0$–1 effective excitation temperature which contributes to the line intensity is higher than those of $F=2$–1 and $F=1$–1.

When the strong density gradient is present, the LVG approximation fails and an exact radiative transfer calculation is necessary to evaluate the scattering model correctly. Though to evaluate the scattering model exactly is out of the scope in this paper, we can roughly estimate the result of this effect in the context of the LVG model. Most of the emission observed comes from the parts where the optical depth along the line of sight reaches to unity. These regions are different in each hyperfine transition; we make corrections to the effective excitation temperature which contributes the line formation.

Suppose the density distribution in the cloud is given by an inverse law of the radius. If we take the representative density of the cloud 2.2×10^4 cm^{-3} at one position in the LVG model, we can estimate that the effective densities where τ is unity are 9.9×10^3, 9.9×10^3, and 1.1×10^4 cm^{-3}, for the $F=2$–1, 1–1, and 0–1 transitions, respectively. The excitation temperatures of each transition at these points are 4.6, 3.7, and 3.9 K, respectively. Then the observed ratios R_{02} and R_{12}, are 0.61 and 0.55. In this analysis, the steeper density gradient gives higher R_{02}/R_{12}.

TABLE 1. Hydrogen number density ($\times10^4$ cm^{-3}) of the cloud derived from the intensity ratio R_{12}.

Position offset	R.A. (″)		
Dec(″)	30	0	−30
0	2.0	1.6	0.8
−30	1.6	1.6	1.2
−60	1.2	1.6	1.6
−90	1.2	1.6	2.0

For example, a density law as an inverse square of radius gives R_{02}/R_{12} as high as 1.35. Though we do not pursue more serious computations on this model because of the limitation of the LVG model, we believe that most of the intensity anomaly can be interpreted by the scattering effect. However, there are two positions, (0″,−90″) and (−30″,−90″), with an extreme anomaly such as $R_{02}/R_{12} > 1.5$). In order to explain these unusual positions, we need more refined models with steeper density gradient or with clumps. These positions with extreme anomalies are close to IRS11 where OH and H_2O masers and a bipolar flow in CS have been found (Kameya *et al.* 1986; Kameya *et al.* 1990).

We derive the hydrogen density at each position of the cloud from the observed and calculated values of R_{12} and listed them in Table 1. This density corresponds to the outer envelope, and is considered as a lower limit of the density of the cloud which is seen by the HCN $J=1$–0 transition. The inner core derived from the ratio R_{02} is higher by a factor of two than this value. Table I shows that emission of two optically thick hyperfine components $F=2$–1 and $F=1$–1 is formed in the outer envelope with an average density of 1.6×10^4 cm^{-3} at IRS1.

Kameya *et al.* (1986) obtained the hydrogen density 2×10^4 cm^{-3} based on the CS and $C^{34}S$ observations. It seems that the HCN lines are formed outside of the CS emitting region. Table 2 lists the hydrogen densities of NGC 7538 at IRS1 obtained by observations of H_2CO (Boland & de Jong 1981) and NH_3 (Ho *et al.* 1981). The density derived in this paper agrees well with those obtained by other observations within a factor of 2. The minor differences could be due to the uncertainty of the collisional excitation rates used in the calculations for different molecules.

Pratap *et al.* (1989,1990) observed clumps of the cloud with HCO^+ and HCN by the interferometer with an about 3″ beam. They detected 40–50 clumps with a linear scale of about 0.1 pc (5.7″). Though it is interesting to compare our observations with their results, it can be made only at limited positions because they show spectra containing satellite transitions rather at a limited range. Figure 6(a) in Pratap *et al.* (1990) corresponds to the position at the middle between the third and fourth columns of the second row in Fig. 1. Figure 6(a) in Pratap *et al.* seems to indicate that the ratio R_{02}/R_{12} decreases with the right ascencion. This tendency is consistent in our observations in which this ratio varies from 1.05 to 1.00 with a 30″ grid of right ascencion in Fig. 1. The signal-to-noise ratios of Fig. 6(a) in Pratap *et al.* (1990) does not allow us to further discuss

TABLE 2. The hydrogen number densities at NGC 7538 IRS1 derived from observations of molecular lines.

Molecule	Transitions	Density (10^4 cm^{-3})	References
H_2CO	1_{10}–1_{11}	3.0	Boland & de Jong (1981)
NH_3	(1,1) and (2,2)	1.2±0.1	Ho *et al.* (1981)
CS,$C^{34}S$	1–0	2.0	Kameya *et al.* (1986)
HCN	1–0	1.6	This paper

the anomaly. Though it is difficult to assess how strong the HCN clumps found by Pratap *et al.* (1990) influence the observations with larger beam of 22″, the presence of clumps is at least consistent with the indication of the steep density gradient in the cloud.

5. CONCLUSION

In this paper we have presented the results of the HCN observations and calculations for the NGC 7538 molecular cloud. Our calculations use the LVG model, and the line overlapping and scattering effects are taken into account. The conclusions are summarized as follows.

(1) The excitation temperatures of the three hyperfine transitions are not identical due to the differences of radiation trapping and line overlapping of the $J=2$–1 transition. The simple LTE approximation is unrealistic for the NGC 7538. The non-LTE condition causes so-called anomalies.

(2) The ratio of the intensities of the components of the $J=1$–0 transition in the NGC 7538 molecular cloud are strongly influenced by the local line overlapping between the hyperfine components. Due to this overlapping effect, the intensity ratios, R_{02} and R_{12}, decrease.

(3) Considering the scattering effect, the hyperfine components of $F=2$–1 and $F=1$–1 are formed in the outer envelope due to the large opacities, and the $F=0$–1 component from the inner core and outer envelope of NGC 7538 molecular cloud due to the smaller opacity.

(4) Numerical calculations show that the $F=2$–1 and $F=1$–1 components come from an outer envelope with an average density of 1.6×10^4 cm^{-3}. This density is slightly lower than the density of regions derived from CS $J=1$–0 and H_2CO 1_{10}–1_{11} observations.

We gratefully acknowledge NRO for providing Y.X.C. with the telescope time and a financial support. We also thank the colleagues of the VAX computer center at PMO for offering the facility for computation. The Q.Z.'s work is supported by the Chinese Natural Science Foundation Committee.

REFERENCES

Cernicharo, J., Castets, A., Duvert, G.,& Guilloteau, S. 1984, A&A, 139, L13
Boland, W., & de Jong, T. 1981, A&A, 98, 149
Dickel, H. R., Dickel, J. R., & Wilson, W. J. 1981, ApJ, 250, L43
Goldreich, P., & Kwan, J. 1974, ApJ, 189, 441
Gottlieb, C. A., Lada, C. J., Gottlieb, E. W., Lilley, A. E., & Litvak, M. M. 1975, ApJ, 202, 655
Guilloteau, S., & Baudry, A. 1981, A&A, 97, 213
Herbst, E., & Klemperer, W. 1973, ApJ, 185, 505
Ho, P. T. P., Martin, R. N., & Barrett, A. H. 1981, ApJ, 246, 761
Kameya, O. 1985, Ph. D. thesis (Tohoku University)
Kameya, O., Hasegawa, T. I., Hirano, N., Tosa, M., Taniguchi, Y., Takakubo, K., & Seki, M. 1986, PASJ, 38, 793
Kameya, O., Morita, K., Kawabe, R. & Ishiguro, M. 1990, ApJ, 355, 562
Kwan, J. 1974, ApJ, 195, L85
Maki, A. G. 1974, J. Phys. & Chem. Ref. Data 3, 221
Monteiro, T. S., & Stutzki, J. 1986, MNRAS, 221, 33
Pratap, P., Batrla, W., & Snyder, L. E. 1989, ApJ, 341, 832
Pratap, P., Batrla, W., & Snyder, L. E. 1990, ApJ, 351, 530
Schwartz, P. R., Cheung, A. C., Bologna, J. M., Chui, M. F., Waak, J. A., & Matsakis, D. 1977, ApJ, 218, 671
Thronson, Jr., H., & Harper D. A. 1979, ApJ, 230, 133
Varshalovich, D. A., & Khersonsky, V. K. 1977, ApL, 18, 167
Walmsley, C. M., Churchwell, E., Nash, A., & Fitzpatrick, E. 1982 ApJ, 258, L75
Zeng, Q., & Lou, G. F. 1988, A&A, 206, 117
Zinchenko, I. I., & Pirogov, L. E. 1987, Astron. Zh., 64, 483